JOURNAL OF MATERIALS SCIENCE 10 (1975) 290–299

Crystal growth of the primary silicon in an Al–16 wt % Si alloy

K. KOBAYASHI, P. H. SHINGU, R. OZAKI
Department of Metal Science and Technology, Kyoto University, Kyoto, Japan

Studies on the crystallographic growth habit of primary silicon crystals in an Al–16 wt % Si alloy were carried out by X-ray micro focus Laue analysis and ECP (electron channelling pattern) analysis.

The plate-like primary silicon crystals grow by the same mechanism as that for germanium dendrites, i.e. the TPRE (twin plane re-entrant edges) mechanism.

The spherical primary silicon crystal in sodium treated melts is composed of several pyramidal grains with tops at the centre of the sphere. Many of these grains have a twin relation to each other. The sodium enriched regions are found at the boundaries of these pyramidal silicon grains.

The external surfaces of the spherical primary crystals exhibit regular crystal facets. The surface facets are most frequently parallel to {111} plane but there are also some facets parallel to other less densely packed planes such as {100}, {211} and so on.

1. Introduction

The crystallographic growth habit of primary silicon crystals in hyper-eutectic Al–Si alloys is changed markedly by the addition of small amount of sodium, i.e., by the so called sodium treatment. The primary silicon crystals in untreated alloys have hexagonal plate-like shape whereas in sodium treated alloys these have spherical shape. Many studies [1-5] on the shape of primary silicon crystals have been carried out by optical microscope and scanning electron microscope, but, up to the present, the studies are limited to the external characteristics. In order to clarify the growth mechanisms of primary silicon crystals, however, the knowledge of crystallographic structure such as grain size and shape, habit plane indices, grain boundary orientation, etc. must be obtained.

The purpose of this paper is to investigate the crystallographic growth habit of primary silicon crystals by X-ray micro focus Laue analysis and ECP (electron channelling pattern) analysis using SEM (scanning electron microscope). The distribution of sodium in the spherical primary

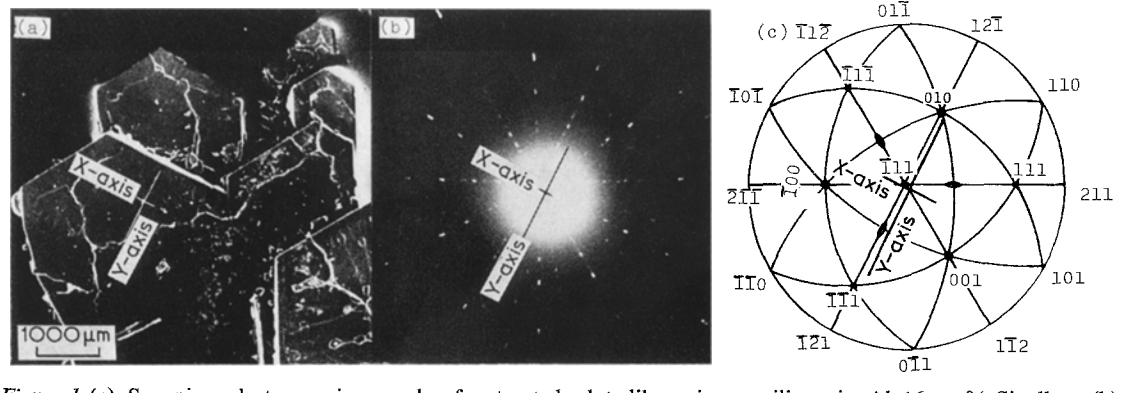

Figure 1 (a) Scanning electron micrograph of extracted plate-like primary silicon in Al–16 wt % Si alloy. (b) X-ray diffraction Laue pattern of a spot indicated by a cross in (a). (c) Stereographic projection with the X-ray incident beam direction as the projection pole.

silicon crystals is studied by EPMA (electron probe microanalysis). The results will be discussed in connection with the growth mechanisms of primary silicon crystals in untreated and sodium treated Al–Si alloys.

2. Experimental

A master alloy containing about 16 wt% of silicon was prepared using 99.99 % pure aluminium and high purity silicon (better than 99.999 %). In each experimental run, 30 g of the alloy was placed in a high purity alumina crucible and remelted at 850 °C in a vertical resistance furnace. Then the specimens were solidified under a cooling condition of 2 °C min^{-1}. The sodium treatment was performed by covering the melts with a mixture of NaF and NaCl.

Optical microscope observation of solidified

Figure 2 Scanning electron micrograph of growth front of extracted primary silicon showing multiple twin traces in Al–16 wt % Si alloy.

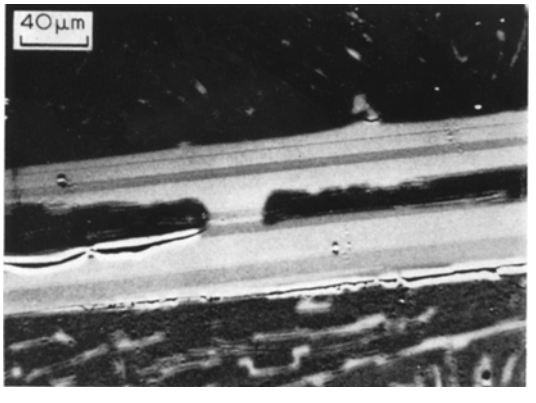

Figure 3 Back-scattered electron scanning image of a polished surface of primary silicon crystal showing the existence of multiple twinning.

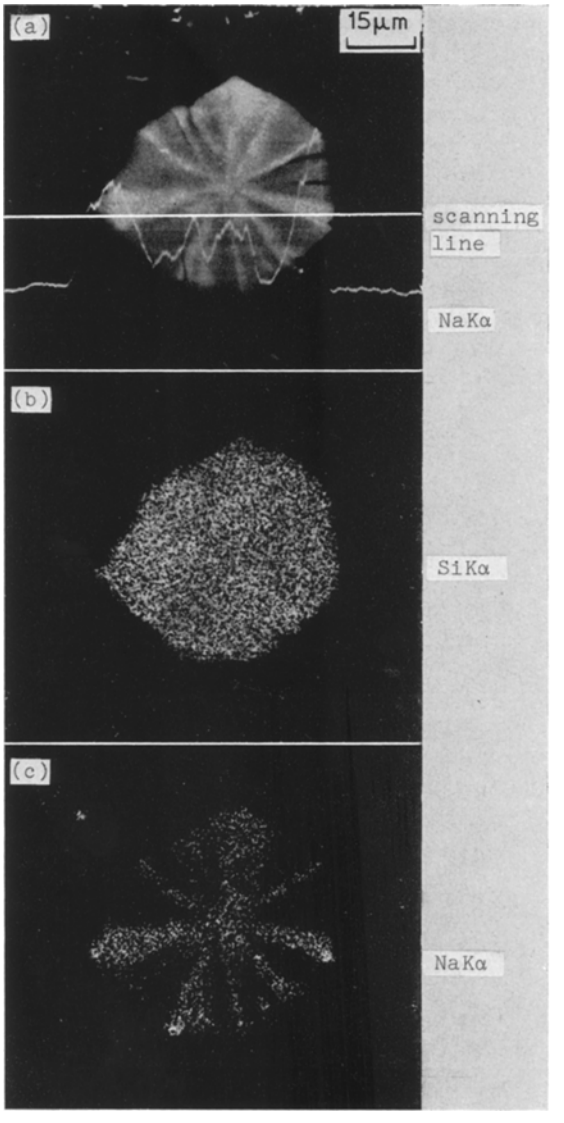

Figure 4 Electron scanning images of the spherical primary silicon crystal in an Al–16 wt % Si alloy treated with sodium. (a) Back-scattered electron scanning image (b) Si$K\alpha$ electron scanning image. (c) Na$K\alpha$ electron scanning image. Note that the contrast in (a) matches the sodium segregated region revealed in Na$K\alpha$ image (c).

structure, EPMA analysis for the sodium distribution examination and ECP analysis for crystallographic orientation determination were performed on the polished sections of the specimens. The X-ray micro focus Laue analysis was performed on extracted primary silicon crystals for the studies on the crystallographic growth habit, i.e., the indices of growth plane, possible growth orientation and the relative orientation relationships between adjacent grains within one primary particle.

The size of the electron beam diameter for ECP analyses was 10 μm (at 50 kV acceleration). In the case of microfocus X-ray analyses, the size of the incident beam (Cu target at 50 kV acceleration) diameter was 50 μm.

3. Results and discussion

3.1. Plate-like primary silicon crystals grown from untreated melts

The typical shape of the primary silicon crystals is hexagonal plates as shown in Fig. 1a. The angles of the corners of the plates are either 120° or 240°. The Laue pattern of the plate-like silicon in Fig. 1a with the incident X-ray direction perpendicular to the surface of the plate is shown in Fig. 1b, and its stereographic projection is given in Fig. 1c. The stereographic projection shows the following results: the surface of the plate-like silicon crystal is parallel to {1 1 1} plane, the three edges of the plate are parallel to $[\bar{1}0\bar{1}]$, $[\bar{1}\bar{1}0]$ and $[0\bar{1}\bar{1}]$ directions, and the growth directions are $[12\bar{1}]$, $[\bar{1}1\bar{2}]$ and $[\bar{2}\bar{1}1]$. Fig. 2 shows the side plane of a plate-like silicon crystal showing several parallel twin traces running parallel to the edges of the plate. The twin traces are also observed on the polished surfaces of primary silicon crystals in the back-scattered electron images as shown in Fig. 3.

The existence of twin traces along the edges which are parallel to one of ⟨1 1 0⟩ directions suggests that the hexagonal plate grows along ⟨1 1 2⟩ directions by the TPRE mechanism which was reported by Billig [6], Wagner [7] and Hamilton and Seidenticker [8] for the plate-like dendritic growth of germanium crystals.

3.2. Spherical primary silicon crystals grown from sodium treated melts

3.2.1. Sodium distribution

It is well known that a high sodium addition produces spherical primary silicon. Several investigations on the distribution of sodium in the solidified structure of Al–Si alloys have been reported [2, 9], however, the detailed distribution of sodium within the primary silicon crystal has not been studied. In the present study,

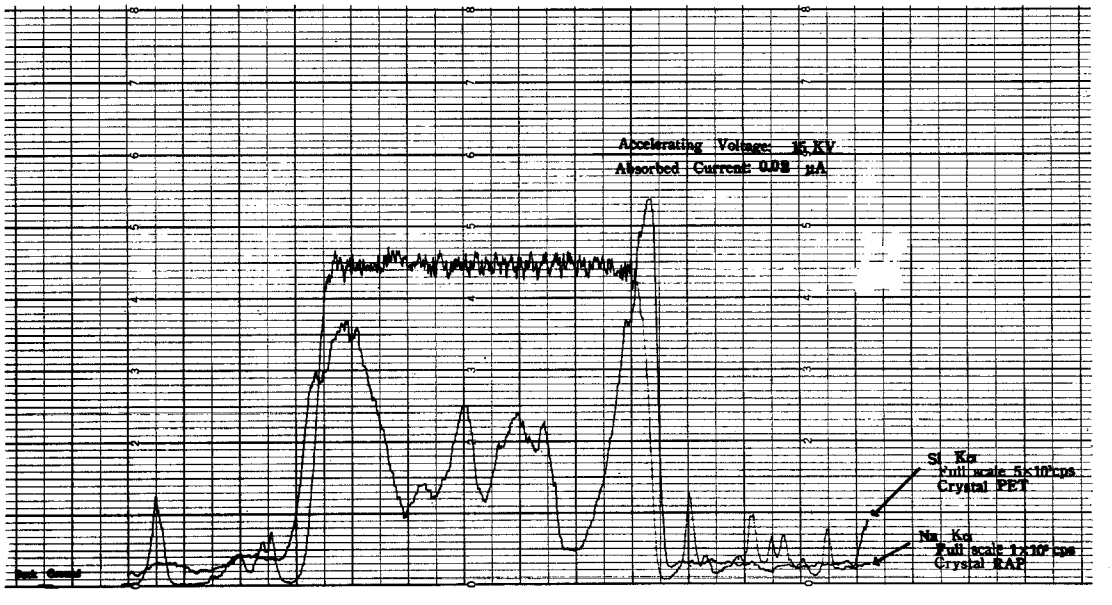

Figure 5 Electron microprobe line traces for Si$K\alpha$ and Na$K\alpha$ radiation of the spherical primary silicon crystal in Fig. 4.

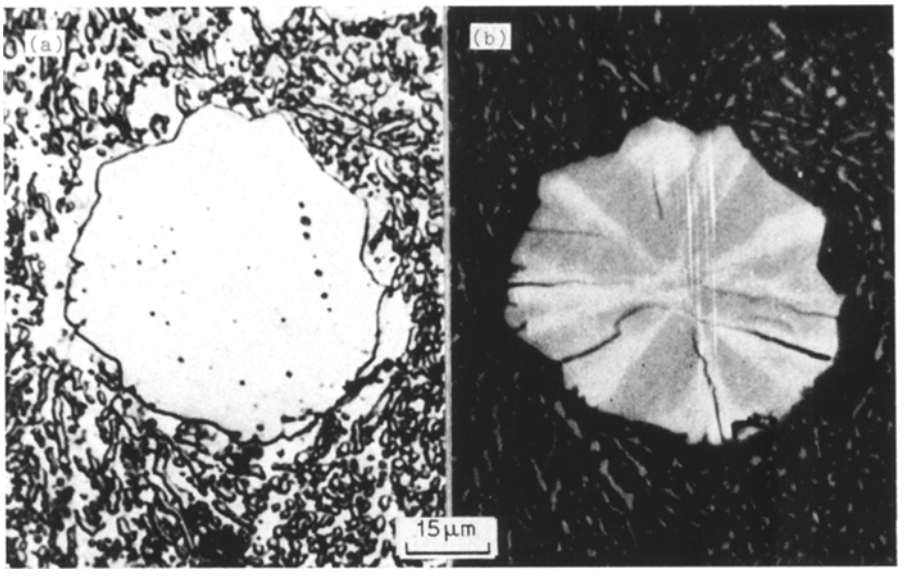

Figure 6 (a) Photomicrograph of spherical primary silicon crystal in Al–16 wt % Si alloy treated with sodium. (b) Back-scattered electron scanning image. The polished surface passes through the centre of a sphere. Note that sodium rich bands fan out from the centre to the periphery of the spherical silicon crystal.

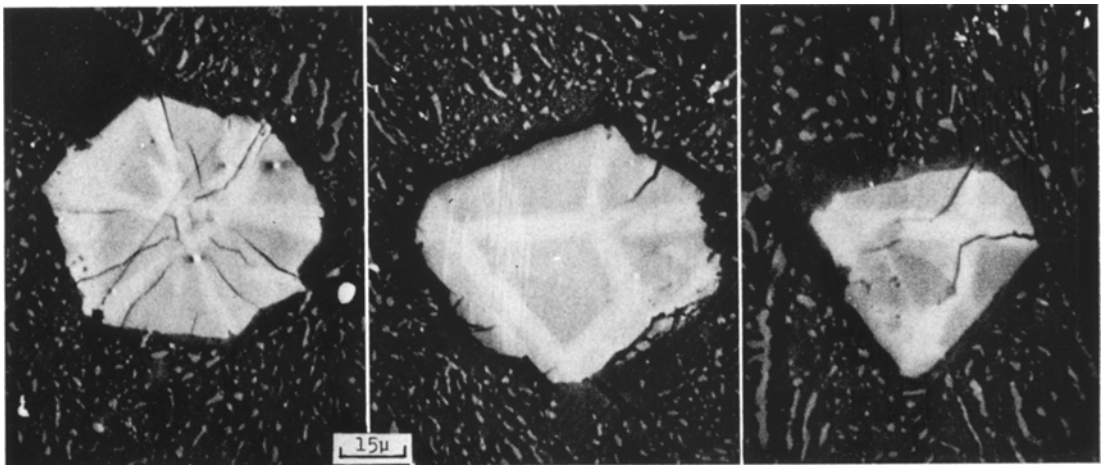

Figure 7 Back-scattered electron scanning images of spherical primary silicon crystals. The polished surface does not pass through the centre of a sphere.

careful EPMA analyses together with the back-scattered electron images showed the existence of sodium enriched regions within a spherical primary silicon crystal. Fig. 4 shows electron scanning images of a spherical primary silicon crystal in an Al–16 wt % Si alloy treated with sodium. Note that the contrast in the back-scattered electron image in Fig. 4a matches the sodium segregated region revealed in the Na$K\alpha$ image in Fig. 4c. The backscattered electron image can thus be used for the identification of the sodium enriched regions in spherical silicon crystals. The electron microprobe line traces for Si$K\alpha$ and Na$K\alpha$ radiations of the spherical primary silicon crystal in Fig. 4a are shown in Fig. 5. Fig. 6 shows a photomicrograph and a back-scattered electron image of a spherical silicon when the polished surface passes through

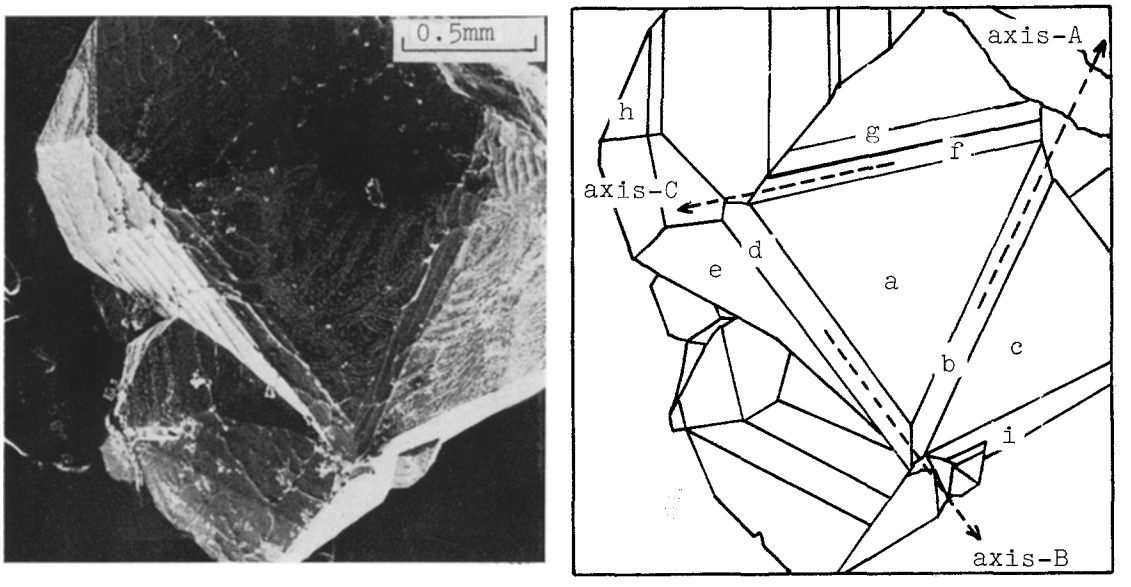

Figure 8 Scanning electron micrograph of an extracted primary silicon particle in Al–16 wt % Si alloy with large additions of sodium, and its schematic figure illustrating the crystal facets examined by X-ray diffraction analyses.

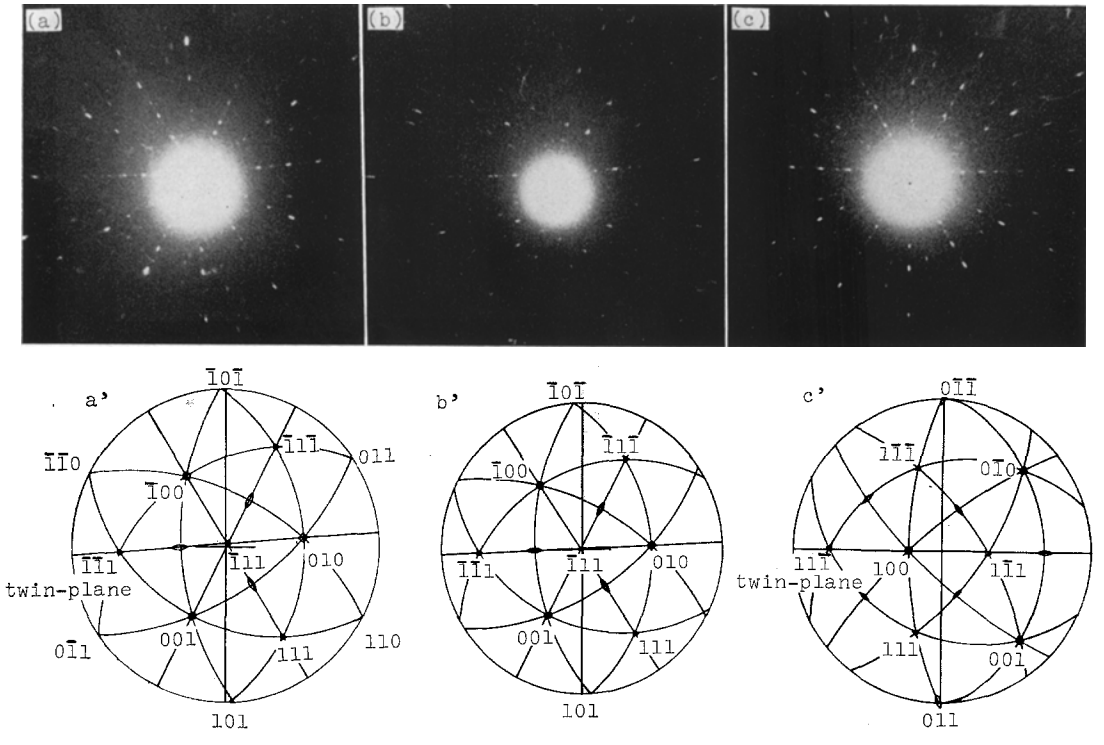

Figure 9 (a), (b) and (c) are X-ray Laue patterns from the silicon particle with incident beam direction parallel to the surface normals of planes (a), (b) and (c) in Fig. 8 respectively. The silicon particle is rotated about *A*-axis indicated in Fig. 8. The stereographic projections a′, b′ and c′ show the crystal orientations derived from the Laue patterns. (a) (b) and (c) above with the surface normal of surface (a) in Fig. 8 as the projection pole.

the centre of the sphere. The sodium enrichments are seen in narrow regions which spread wider from the centre to the periphery of the spherical silicon. Fig. 7 shows back-scattered electron images when the polished surfaces do not pass through the centre of the spheres. The sodium rich regions in these cases are not observable at the centres of the silicon spheres.

The cracks in silicon crystals observed in Figs. 4 and 6 which spread from the centre to the periphery indicate the accumulation of stress in the tangential direction of the primary silicon spheres. The high concentration of sodium at the boundaries of pyramidal crystal grains revealed in the present investigation may suggest that the stress accumulation is relaxed by the sodium atoms.

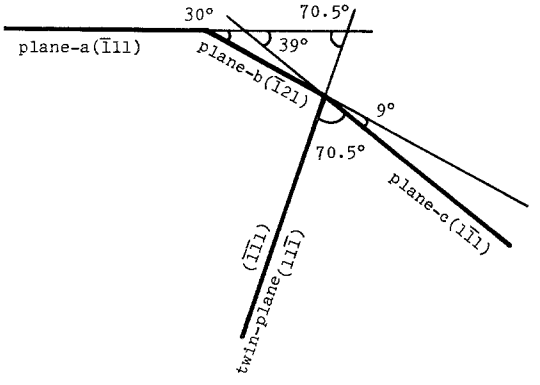

Figure 10 Cross-sectional illustration showing the angular relationships between a twin plane and facets (a), (b) and (c). The plane of the paper is perpendicular to the *A*-axis in Fig. 8.

3.2.2. Micro focus X-ray diffraction analyses

Fig. 8 shows a scanning electron micrograph of an extracted primary silicon crystal in sodium treated Al–16 wt% Si alloy and its schematic figure illustrating the crystal facets examined by X-ray diffraction analyses. X-ray Laue patterns were taken with the incident beam direction parallel to the surface normals of facets (a)-(i) in Fig. 8. The facets (a)-(i) are found to belong to one crystal grain with the exceptions of (c) and (i). These two facets belong to a grain which has a twin relation with the grain to which the other facets belong. Fig. 9a, b and c are X-ray Laue patterns from facets (a), (b) and (c) in Fig. 8, respectively, when silicon particle is rotated about the *A*-axis indicated in the photograph.The indices of these facets were determined from the measured angular relationships together with the orientation analyses by the Laue patterns. The angles between facets were measured with a reflection goniometer. The indices for the facets (a)-(i) were determined as,

$$a//(\bar{1}11) \quad d//(\bar{1}12) \quad g//(\bar{5}11)$$
$$b//(\bar{1}21) \quad e//(001) \quad h//(\bar{1}\bar{1}1)$$
$$c//(1\bar{1}1) \quad f//(\bar{3}11) \quad i//(001)$$

The stereographic projections a′, b′ and c′ show the crystal orientations determined from the Laue patterns (a), (b) and (c) in Fig. 9 with the surface normal of surface (a) in Fig. 8 as a projection pole. A cross-sectional illustration

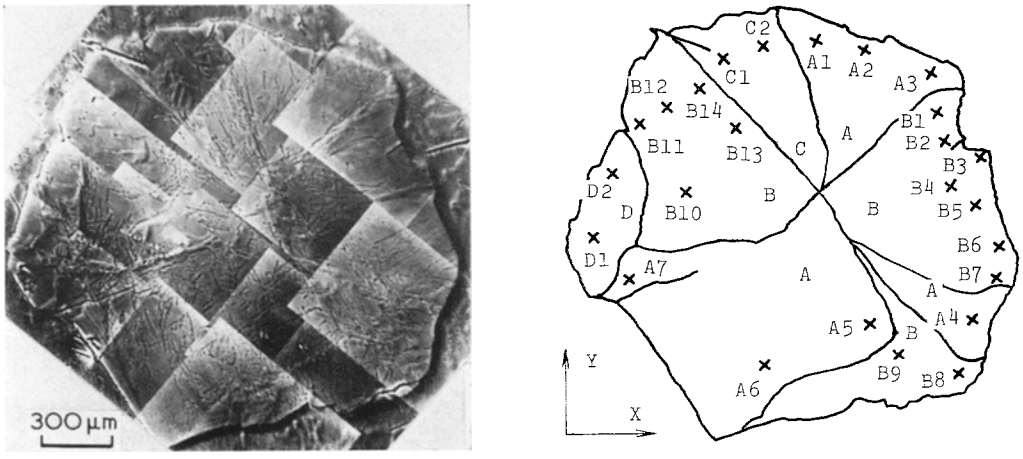

Figure 11 Back-scattered electron scanning image of the spherical primary silicon crystal in an Al–16 wt% Si alloy treated with sodium and its schematic figure showing the positions analysed with ECPs obtained using the scanning electron microscope. Crosses indicate the positions analysed with ECP.

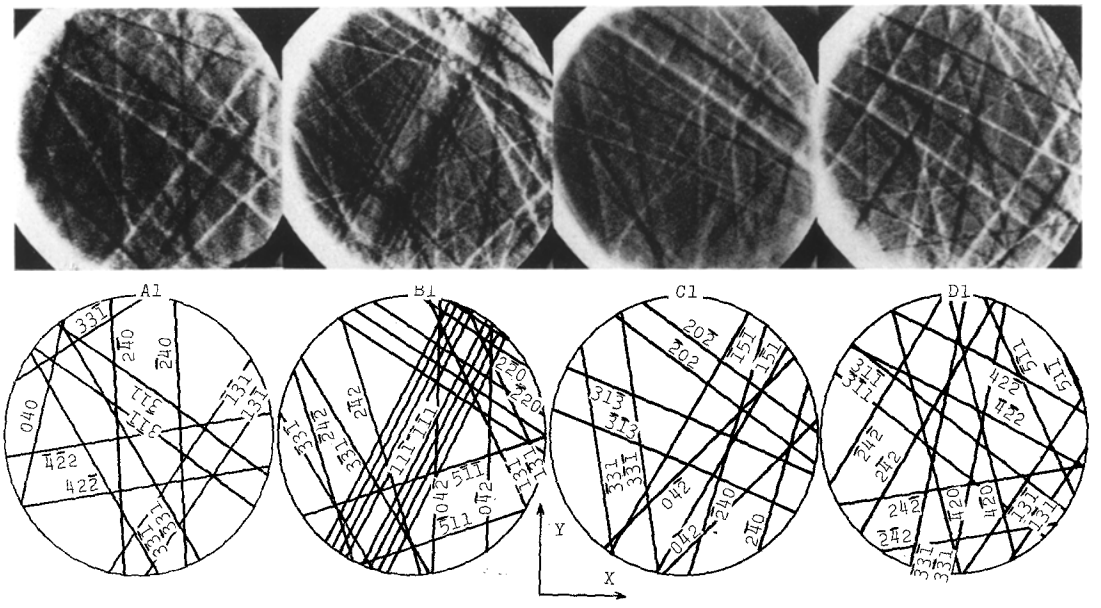

Figure 12 Electron channelling patterns for 50 kV electrons obtained from the positions indicated in Fig. 11 and the corresponding ECP maps.

in Fig. 10 shows the angular relationships between a twin plane and facets (a), (b) and (c) when the plane of the paper is perpendicular to the A-axis in Fig. 8. The twin plane passes through the centre of the spherical silicon crystal and the direction of A-axis is $[\bar{1}0\bar{1}]$ for facet (a) or $[0\bar{1}\bar{1}]$ for facet (c) and the angles between the twin plane and facet (a) or (c) are both 70.5°.

3.2.3. Electron channelling pattern analyses

Fig. 11 shows a back-scattered electron scanning image of a spherical primary silicon crystal in an Al–16 wt % Si alloy treated with sodium and its schematic drawing showing the positions ana-

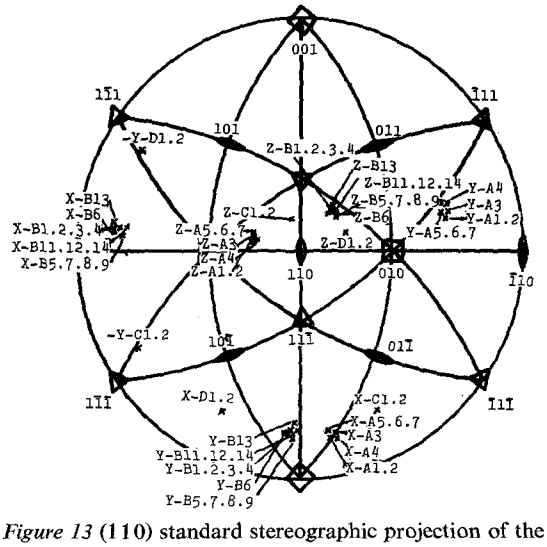

Figure 13 (110) standard stereographic projection of the spherical primary silicon crystal, showing the orientations of X, Y, Z analysed with ECPs which are obtained from the positions indicated in Fig. 11.

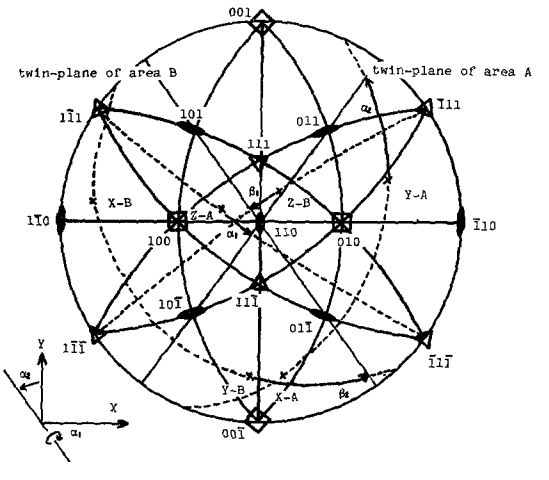

Figure 14 (110) standard projection indicating the relative orientation of crystals A and B determined from ECP maps of Fig. 12. $\alpha_1(=\beta_1)$ is the angle between the twin plane and Z-axis. $\alpha_2(=\beta_2)$ is the angle between the twin trace on X-Y plane and Y-axis.

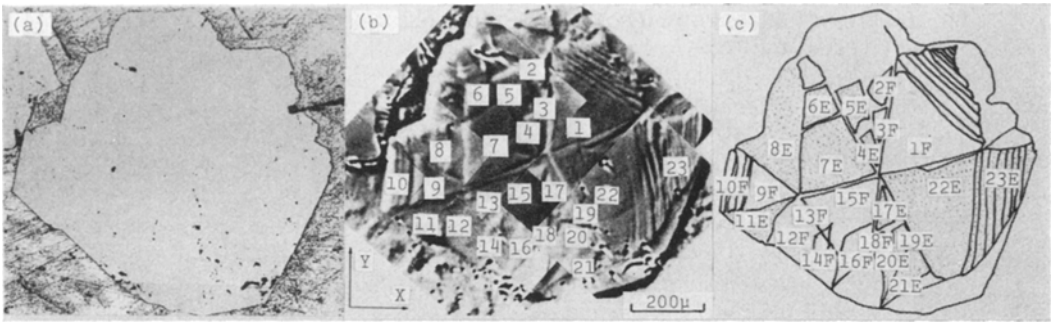

Figure 15 (a) Photomicrograph of the spherical primary silicon crystal treated with sodium. (b) Back-scattered electron scanning image. Numbers on the photograph indicate the positions analysed with ECP. (c) Schematic figure of (b) showing the regions of two different crystal orientation (indicated by E and F) revealed by ECP analyses.

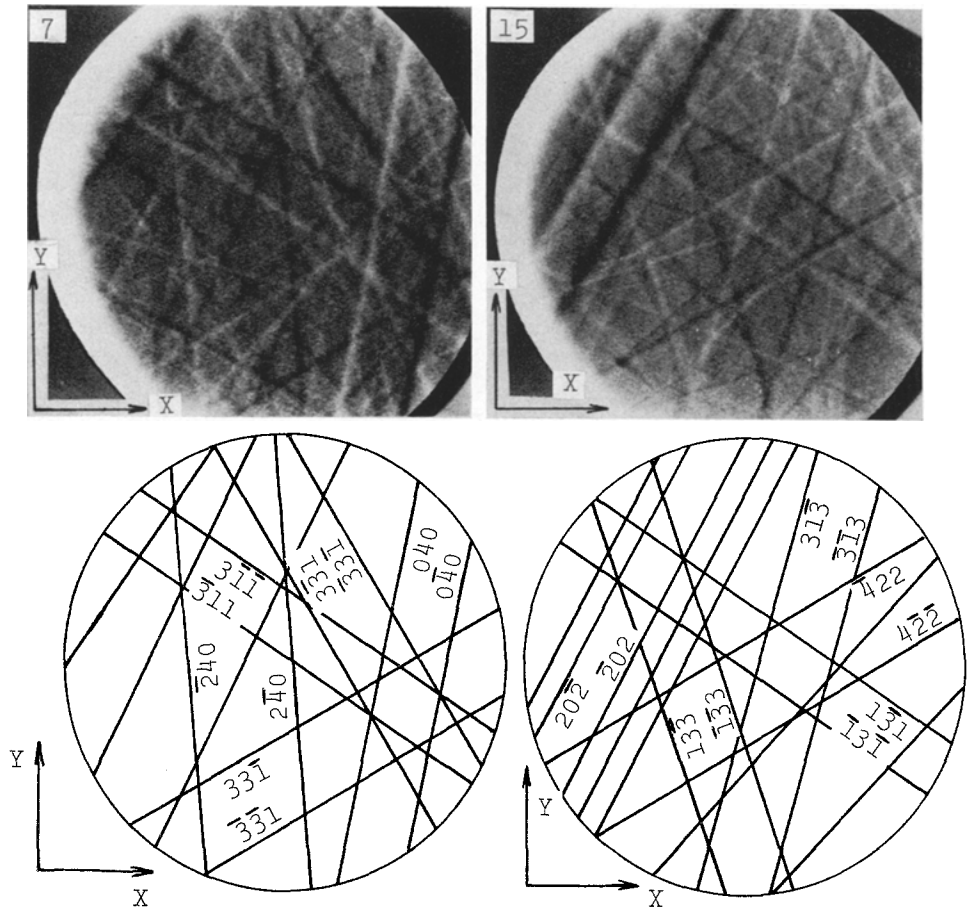

Figure 16 Electron channelling patterns for 60 kV electrons obtained from the positions indicated in Fig. 15 and corresponding ECP maps.

lysed with the electron channelling patterns (ECPs). The ECPs obtained from the positions A1, B1, C1 and D1 indicated in Fig. 11 and the corresponding ECP maps are shown in Fig. 12. Fig. 13 shows (110) standard stereographic projections, for positions indicated by crosses in

Fig. 11, obtained from ECP analyses. The X, Y and Z directions fixed to the spherical primary silicon particle, indicated in Fig. 11, are shifted into four different groups indicating that this primary silicon particle contains four differently oriented crystal grains. On Fig. 13, X-, Y- and Z-axes of crystal A can be matched with X-, Y- and Z-axes of crystal B by a 109.5° rotation about [1 1 0] axis which is common to both crystals. The same orientation relationship exists for crystals B and C. Crystal A and crystal D can be matched by rotating 60° around a common [1 1 $\bar{1}$] axis. By a crystallographic consideration as reported in a previous work [10], these results show that there are three pairs of twin relations in this silicon particle, namely, A-B, B-C and A-D. Fig. 14 shows (1 1 0) standard projection indicating the relative orientation of crystals A and B determined from ECP maps of Fig. 12. The twin planes of A and B crystals are ($\bar{1}$ 1 $\bar{1}$) and (1 $\bar{1}$ $\bar{1}$) respectively. $\alpha_1(= \beta_1 \cong 15°)$ is the angle between the twin plane and Z-axis. $\alpha_2(= \beta_2 \cong 35°)$ is the angle between the twin trace on X-Y plane and Y-axis. From these results it is found that the line on Fig. 11 which runs from upper left side to lower right side corresponds to the trace of the {1 1 1} twin plane separating A and B crystals and the line which runs from upper right side to lower left side corresponds to a grain boundary which is nearly parallel to {2 1 1} plane common to A and B crystals.

Another example of spherical primary silicon crystal is shown in Fig. 15a (photomicrograph), b (back-scattered electron scanning image) and c (schematic drawing). It is to be noted that no twin trace nor grain boundary is observable under an optical microscope, whereas in the backscattered electron scanning image, many twin traces are revealed. Numbers on Fig. 15b indicate the positions analysed with ECPs. The letters E and F in Fig. 15c indicate the regions of two different crystal orientations revealed by ECPs. Typical ECPs (obtained from the positions 7 and 15 in Fig. 15) and corresponding ECP maps are shown in Fig. 16. These maps are analysed to give a standard (1 1 0) projection given in Fig. 17 which shows that crystals E and F have a twin relationship. $\gamma_1(= \delta_1 \cong 15°)$ is the angle between the twin plane and Z-axis. $\gamma_2(= \delta \cong 25°)$ is the angle between the twin trace on X-Y plane and Y-axis.

Some of the primary silicon crystals showed more complicated back-scattered electron scanning images. An example of such cases is shown in Fig. 18. The ECP analyses on positions indicated by the numbers 1-8 in Fig. 18 revealed the twin relations between positions 2-3 and 6-7 It was found that there is a common crystallo-

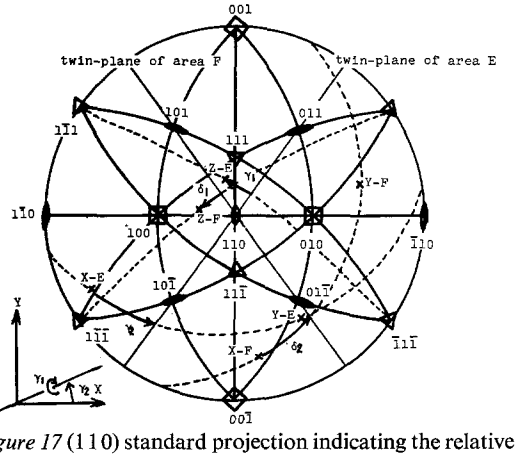

Figure 17 (1 1 0) standard projection indicating the relative orientation of crystals E and F determined from ECP maps of Fig. 16. $\gamma_1(= \delta_1)$ is the angle between the twin plane and Z-axis. $\gamma_2(= \delta_2)$ is the angle between the twin trace on X-Y plane and Y-axis.

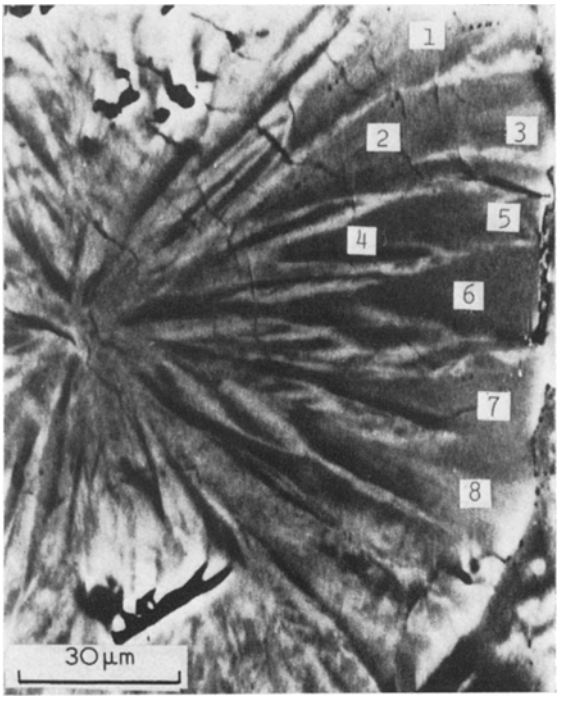

Figure 18 Back-scattered electron scanning image of a spherical primary silicon crystal treated with sodium. Numbers on the photograph indicate the positions analysed with ECP.

graphic relationship between positions 1-2, 1-3, 2-4 and 4-6. A rotation of approximately 30° about a common ⟨2 1 1⟩ direction.

The spherical growth of silicon crystals in sodium treated melts is caused by the lack of re-entrant twins (due probably to the poisoning by sodium) in the spherical silicon. When the re-entrant twin mechanism of growth is no longer operative, the growth would proceed in an isotropic way causing spherical shape of primary crystals. In the case of growth in a spherical shape, slow growing low energy planes would tend to appear as facets. The occurrences of growth twinnings which are frequently found in the present study may help the low energy planes to appear as facets.

4. Conclusions

A study on the crystallographic growth habit of primary silicon crystals, by X-ray micro focus Laue analyses and ECP analyses, was carried out. The results obtained are as follows:

(1) The plate-like primary silicon crystal in hyper-eutectic Al–Si melt grows by the same mechanism as that for the plate-like dendritic growth of germanium, i.e., the TPRE (twin plane re-entrant edges) mechanism.

(2) The external surface of the spherical primary crystals exhibits regular crystal facets. The surface facets are most frequently parallel to {1 1 1} plane but there are also some facets parallel to other less densely packed planes such as {1 0 0}, {2 1 1} and so on.

(3) The spherical primary silicon crystal is composed of several pyramidal grains with the tops at the centre of the sphere. The sodium enriched regions are found at the boundaries of these pyramidal grains and many of these grains have twin relations to each other.

Acknowledgements

The authors are grateful to Dr N. Narita for discussions on the crystallographic relationships. Our thanks are also due to Mr T. Yamamoto of JEOL Ltd. for the use of a scanning electron microscope with electron channelling and micro analysis attachments.

References

1. I. OBINATA and N. KOMATSU, *Sci. Rep. Research Inst. Tohoku Univ.* **A9** (1957) 107.
2. V. L. DAVIS and R. W. WEST, *J. Inst. Metals* **92** (1963-64) 175.
3. C. B. KIM and R. W. HEINE, *ibid* **92** (1963-64) 367.
4. M. G. DAY, *Nature* **219** (1968) 1357.
5. H. FREDRICKSSON, M. HILLERT and N. LANGE, *J. Inst. Metals* **101** (1973) 285.
6. E. BILLIG, *Proc. Roy. Soc.* **A229** (1955) 346.
7. R. S. WAGNER, *Acta Met.* **8** (1960) 57.
8. D. R. HAMILTON and R. G. SEIDENSTICKER, *J. Appl. Phys.* **31** (1960) 1165.
9. R. C. PLUMB and J. E. LEWIS, *J. Inst. Metals* **86** (1957-58) 393.
10. K. KOBAYASHI, P. H. SHINGU and R. OZAKI, *J. Japan Inst. Metals* **38** (1974) 338.

Received 24 July and accepted 28 August 1974.